

Strengthening Supersolids with Disorder in the Extended Bose-Hubbard Model

Fei Lin^{1,2}, T. A. Maier³, and V. W. Scarola¹

¹*Department of Physics, Virginia Tech, Blacksburg, Virginia 24061, USA*

²*Department of Physics and Engineering, Washington and Lee University, Lexington, Virginia 24450, USA and*

³*Computer Science and Mathematics Division and Center for Nanophase Materials Sciences, Oak Ridge National Laboratory, Oak Ridge, Tennessee 37831, USA*

(Dated: October 2, 2015)

The extended Bose-Hubbard model captures the essential properties of a wide variety of physical systems including ultracold atoms and molecules in optical lattices, josephson junction arrays, and narrow band superconductors. It exhibits a rich phase diagram including a supersolid phase where a lattice solid coexists with a superfluid. We use quantum Monte Carlo to map out the phase diagram of the extended Bose-Hubbard model on the simple cubic lattice where the supersolid is expected. We find that the supersolid is very delicate because unexpected phase separated states compete with the supersolid. We add disorder to the extended Bose-Hubbard model and find that the supersolid phase is enhanced by disorder as phase separation is suppressed. Our results establish optimal regimes for observing supersolids and therefore have important implications for their observation.

PACS numbers: 67.80.kb, 67.80.dj, 71.23.An, 67.25.dj

I. INTRODUCTION

A superfluid and a solid can, in principle, coexist in the same place at the same time. This unique state of matter, a supersolid, has not been conclusively identified in the laboratory to date even though it was proposed more than 45 years ago in the context of superfluid ⁴He [1, 2]. ⁴He experiments discussing possible observation of a supersolid have remained controversial [3, 4].

Lattice models of supersolids (the extended Bose-Hubbard model [5] in particular) were used to study the critical properties of the supersolid phase of ⁴He [6, 7]. But subsequent work showed that these lattice models capture the essential properties of many other physical systems, including ultracold atoms and molecules in optical lattices [8–13], josephson junction arrays [14, 15], and narrow-band superconductors [16]. The latter connection can be made rigorous via a direct mapping between local Cooper pairs and bosons. The supersolid of bosons in this case maps to coexisting superconducting and charge density wave order which has been of interest in a variety of compounds, e.g., BaBiO₃ doped with K or Pb [17].

Work on lattice models suggest that supersolids should be rather delicate and therefore difficult to observe. In two dimensions (2D) it is now known that the supersolid competes with phase separation. A mean-field argument [18] shows that the formation of domain walls favors phase separation because (for low coordination number) the domain wall intrinsic to the phase separated state gains in kinetic energy. But on lattices with higher coordination number, e.g., the triangular lattice, quantum Monte Carlo (QMC) calculations show [19] that phase separation is suppressed and the supersolid state gains in energy.

Furthermore, QMC results show that lattice supersolids in 2D are also highly susceptible to disorder. Results on the square lattice [20] show that spatial disorder

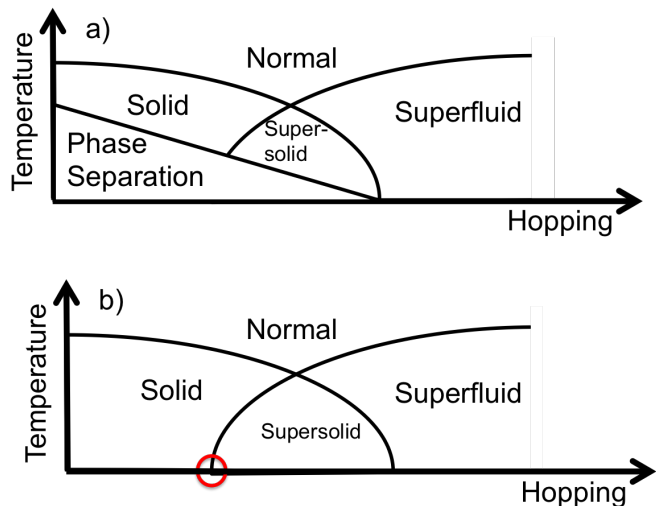


FIG. 1. a) Schematic of the phase diagram we find for the extended Bose-Hubbard Model in the absence of disorder on the simple cubic lattice and at fixed chemical potential. The phase separated regime is unexpected. b) Schematic of the expected [11, 14, 22] phase diagram. The circle denotes a quantum critical point separating the solid and the supersolid phases with no phase separation. Remarkably, we find that the addition of weak on-site disorder produces a phase diagram similar to the bottom panel. But crucial differences emerge at the boundary of the solid phase. In the thermodynamic limit the solid phase should be bounded by a Griffiths-type phase in the presence of disorder [23, 24]. This would also eliminate the conventional quantum critical point denoted by the circle.

destroys the solid itself leaving no chance for the supersolid. This problem stems from an Imry-Ma-type mechanism [20, 21] implying that the solid is unstable in the presence of arbitrarily weak disorder in less than three dimensions (3D).

In 3D we expect a solid to be robust against disorder because the Imry-Ma mechanism is avoided [25]. Furthermore, high coordination numbers have been shown to suppress phase separation on the simple cubic lattice. QMC results [22] (in the absence of disorder) report a strong supersolid and no phase separation. 3D lattice models therefore seem to be the best arena to study supersolid behavior.

Study of the extended Bose Hubbard model in 3D has become more pressing because of recent work [13] that has successfully demonstrated placement of bosonic chromium atoms in a cubic optical lattice. The atoms have a magnetic dipole moment. When polarized these moments induce long range interactions. A theory-experiment comparison [13] shows that the extended Bose-Hubbard model quantitatively captures the physics of this system thus paving the way for the possibility of a direct observation of a supersolid.

We use QMC to revisit the stability of the lattice supersolid in the simple cubic lattice. We study the phase diagram of the extended Bose-Hubbard model. Our primary results are summarized in Fig. 1. Our results show that the extended Bose-Hubbard model does in fact show phase separation at low temperature in some parts of the phase diagram (See Fig. 1a). This is in contrast to work in Ref. 22 that did not find evidence for phase separation. Our methods differ by going to large system sizes, lower temperature, and by using a histogram analysis (discussed herein) to identify phase separation. The phase separated state found here shows that the solid and the supersolid do *not* meet at a quantum critical point as is widely believed (See Fig. 1b).

We also include disorder in our study to examine the stability of the supersolid. We find that disorder suppresses phase separation. We map out the finite disorder phase diagram to find that the absence of phase separation leaves the phase diagram to resemble the phase diagram previously expected in the disorder-free case (Fig. 1b). But there are important differences between the phase diagrams previously expected for the extended Bose-Hubbard model without disorder and the phase diagram we find in the presence of disorder. Most significantly, the theorem of inclusions [23, 24] implies that the transition between the solid and the supersolid should be mediated by a Griffiths regime and not a conventional quantum critical point. We also find that disorder enhances the supersolid critical temperature [25]. We use systematic finite-size scaling to show that increasing disorder increases the critical temperature of the supersolid. Our results therefore indicate that supersolids in the extended Bose-Hubbard model are unexpectedly susceptible to phase separation on the simple cubic lattice but are favored (and even enhanced) for a moderate amount of disorder.

The plan of the paper is as follows. In Sec. II we discuss relevant parameter regimes of the extended Bose-Hubbard model and mean field estimates of the phase diagram. In Sec. III we map the attractive Fermi-Hubbard

model to a model of repulsive bosons. This mapping shows that our results can be considered in the context of magnetic polarons, short coherence length type II superconductors, and, more generally, narrow-band superconductors [16]. Sec. IV overviews the numerical methods used to study the phase diagram. Sec. V discusses the order parameters that allow us to define the supersolid and other phases. In Sec. VI we show that the extended Bose-Hubbard model at weak hopping can be understood by mapping to a model known to exhibit phase separation, the classical Blume-Capel model. The mapping supports our finding of phase separation in the extended Bose-Hubbard model on the simple cubic lattice. Sec. VII specifies the nature of the two phase separated states that we find and details the numerical method used to find them. Sec. VIII uses QMC to compute the order parameters in different parameter regimes and identify phases. Sec. IX discusses the finite-size scaling relations used to map out the phase diagram. Sec. X culminates the results of previous sections to construct the finite temperature phase diagram of the extended Bose-Hubbard model for several different disorder strengths. We find that disorder eliminates phase separation from the phase diagram. Sec. XI uses finite-size scaling to compute the supersolid critical temperature as a function of disorder. We find that disorder enhances supersolidity [25]. Sec. XII summarizes our results.

II. MODEL

We study a tight-binding model of repulsive soft-core bosons hopping in a simple cubic lattice of side lengths L with on-site disorder:

$$H = -t \sum_{\langle i,j \rangle} (a_i^\dagger a_j + \text{H.c.}) + \frac{U}{2} \sum_i n_i(n_i - 1) + V \sum_{\langle i,j \rangle} n_i n_j - \sum_i \mu_i n_i, \quad (1)$$

where a_i (a_i^\dagger) is the boson annihilation (creation) operator at site i , $n_i = a_i^\dagger a_i$ is the particle number operator, U is the on-site repulsion, and V is the nearest neighbor repulsion. Here $\mu_i = \mu - \epsilon_i$, where μ is the average chemical potential of the system, and $\epsilon_i \in [-\Delta, \Delta]$ is the on-site disorder potential. We use periodic boundary conditions. Hereafter we will use U as the energy unit and set $k_B = 1$.

For $V = 0$ and $\Delta = 0$ the model reduces to the well known Bose-Hubbard model [26]. At zero temperature there exist two competing phases, an incompressible Mott insulator at low hopping and a superfluid (SF) at large hopping that spontaneously breaks the continuous $U(1)$ gauge symmetry of the model (the phase invariance of the bosonic operators). At fixed μ these phases are separated by a quantum critical point at a critical t .

Including a nearest-neighbor repulsion, $V > 0$, leads

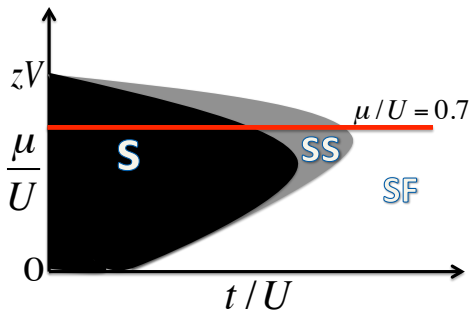


FIG. 2. Schematic of the conventional zero temperature mean field phase diagram of Eq. (1) at density below one. By fixing the chemical potential to be $\mu/U = 0.7$ and increasing the hopping t from zero we traverse the phase diagram through the solid, supersolid, and superfluid phases, respectively. Note that this phase diagram excludes phase separation because it was excluded as a possibility in the mean field analysis [11, 14].

to additional phases. For large V the bosons tend to sit at every other site to form a charge density wave, a solid (S), which spontaneously breaks the \mathbb{Z}_2 sublattice symmetry. When the hopping and interaction terms are comparable a supersolid forms which derives from dual spontaneous symmetry breaking of both the $U(1)$ gauge symmetry and the \mathbb{Z}_2 sublattice symmetry throughout the entire sample. The result is simultaneous superfluid and solid order, a supersolid (SS). To study a regime consistent with spatially decaying interactions and a strong supersolid we choose $zV = U = 1$ [18, 22], where $z = 6$ is the lattice coordination number.

Mean-field analyses of the disorder-free extended Bose-Hubbard model [11, 14, 25] show that the supersolid sits between the solid and the superfluid in the phase diagram. Fig. 2 shows the zero temperature mean field phase diagram in the dilute (low μ) regime with $\Delta = 0$. In the following we select a specific chemical potential, $\mu = 0.7$, unless otherwise stated. The horizontal line indicates that increasing t while keeping $\mu = 0.7$ allows us to transverse three of the phases discussed so far, i.e., $S \rightarrow SS \rightarrow SF$. This choice also keeps the density below one. By adding disorder to phases lying along the horizontal line, we can obtain other intriguing phases, such as, the Bose glass (BG) [26] and a disordered solid (DS) phase. We will also be able to study the interplay of the supersolid with disorder.

We note that phase separation (PS) is another possibility. Phase separation is known to compete with the supersolid, particularly in 2D [18]. But mean-field arguments have shown that phase separation should be suppressed in 3D [18]. We will return to the issue of phase separation in later sections. We will show that PS dominates the low temperature phase diagram (even in the cubic lattice) but that thermal fluctuations and/or disorder tend to suppress phase separation in favor of SS,

S, and SF phases.

III. MAPPING TO THE ATTRACTIVE FERMIO-HUBBARD MODEL

Before we study the extended Bose-Hubbard model with disorder we define an approximate mapping to the attractive Fermi-Hubbard model. The mapping shows that if we think of tightly bound Cooper pairs as bosons we can interpret our results for bosons in a dual language of Cooper pairs. The attractive Fermi-Hubbard model with disorder has been used to capture the essential physics of narrow band superconductors and more generally to study the interplay of disorder and superconductivity [16].

The attractive Fermi-Hubbard model is given by:

$$H_F = -t^F \sum_{\langle i,j \rangle, \sigma} (c_{i,\sigma}^\dagger c_{j,\sigma} + \text{H.c.}) - |U^F| \sum_i n_{i,\uparrow}^F n_{i,\downarrow}^F + V^F \sum_{\langle i,j \rangle} n_i^F n_j^F - \sum_i \mu_i^F n_i^F, \quad (2)$$

where $c_{j,\sigma}^\dagger$ creates a fermion of spin $\sigma \in \uparrow, \downarrow$ at a site j , and $n_j^F = n_{j,\uparrow}^F + n_{j,\downarrow}^F$ is the fermion number operator. The parameters t^F and V^F denote the nearest-neighbor fermion hopping and repulsion, respectively. μ_j^F is the fermion chemical potential which carries a site index to allow for on-site disorder. The U^F term defines an attractive on-site interaction.

Eq. (2) maps to an extended Bose-Hubbard model in the strongly attractive limit [16]. We take the limit: $|U^F| \gg t^F, V^F$. In this limit double occupancies are favored. We can think of each doublon as a locally formed Cooper pair. Cooper pair hopping is a second order process when viewed in terms of the original fermions. To second order in perturbation theory, Eq. (2) reduces to [16]:

$$H_F \rightarrow -\bar{t} \sum_{\langle i,j \rangle} (\bar{b}_i^\dagger \bar{b}_j + \text{H.c.}) + (\bar{t} + 4V^F) \sum_{\langle i,j \rangle} \bar{n}_i \bar{n}_j - \sum_j \bar{\mu}_j \bar{n}_j, \quad (3)$$

where $\bar{b}_i^\dagger \equiv c_{i,\downarrow}^\dagger c_{i,\uparrow}$ and $\bar{b}_i \equiv c_{i,\downarrow}^\dagger c_{i,\uparrow}^\dagger$ create and annihilate hardcore bosons, respectively. The boson number operator is then $\bar{n}_i \equiv \bar{b}_i^\dagger \bar{b}_i$. $\bar{t} = 2(t^F)^2/|U^F|$ is an effective hopping of Cooper pairs. The renormalized chemical potential is: $\bar{\mu} = -2\mu_j^F - |U^F| + z(\bar{t} + 4V^F)$.

Eq. (3) is a disordered extended Bose-Hubbard model but there are difference between Eqs. (1) and (3). The bosons in Eq. (3) are hardcore but in Eq. (1) they are soft core. The two models can then be equated by taking $U \rightarrow \infty$ in Eq. (1) while also requiring a dilute limit. The latter requirement stems from the commutation relations for hardcore bosons: $[\bar{b}_i, \bar{b}_j^\dagger] = (1 - 2\bar{n}_i)\delta_{i,j}$. The commu-

tation relation shows that Eq. (3) maps onto Eq. (1) only for $\langle \bar{n}_i \rangle \ll 1$.

The mapping above shows that we can interpret results derived for bosons in Eq. (1) as approximations to states found in the attractive Fermi-Hubbard model. For example the superfluid and solid order of Eq. (1) map to superconducting and charge density wave order, respectively. With this construction the supersolid state then corresponds to the coexistence of superconductivity and charge density wave orders [16, 27–32]. Our analysis of Eq. (1) will therefore also offer a probe of coexisting superconductivity and charge density wave order in the presence of disorder. For example, as we will show in Sec. XI, disorder actually raises the critical temperature of the supersolid. By appealing to the above mapping our results will therefore show that disorder increases the critical temperature of the coexisting superconductivity and charge density wave state found in Eq. (3). This is consistent with increases in critical temperatures due to disorder found using the Bogoliubov-de Gennes equations on the attractive Fermi-Hubbard model [33].

IV. NUMERICAL METHODS

We solve Eq. (1) using a numerically exact QMC method: the Stochastic Series Expansion representation with directed loop updates [34, 35]. Various physical quantities, either diagonal or off-diagonal, can be calculated according to the path integral formulation of the QMC simulations. We will discuss several key physical quantities in Sec. V when we describe various order parameters for the different phases. Our results are converged with respect to truncation of the boson number, the number of QMC steps, and the number of disorder profiles. Our estimates of order parameters are therefore exact to within Monte Carlo error.

Disorder averaging is a key part of the numerical procedure. We perform several runs over distinct disorder profiles to ensure proper averaging. To ensure convergent disorder averages, we typically run 1000 QMC simulations with different disorder realizations for each set of parameters. We then plot histograms for the resulting measurement of various physical quantities.

We find three types of distributions in our disorder averaging. The most common distribution is a single Gaussian peak without any “fat” tails in the distribution curve. This type of distribution signifies a unique phase for the parameter set. A Gaussian distribution offers fast convergence with respect to the number of disorder realizations. We also find double-peaked Gaussian distributions that imply phase separation. Our QMC simulations usually end up in one of the two phases depending on the initial configuration. In this case, numerical data are sorted according to the two phases and separate averages need to be done, one for each phase. The third type of distribution is a single Gaussian peak but with a “fat” tail. This happens in the BG phase, where our

order parameters do not assume a definite value. In this case physical quantities will have a slow convergence rate with respect to disorder configurations.

A key numerical step taken in this work is to use the histogram method, normally used for disorder averaging, but in the absence of disorder. The histogram method allowed us to identify phase separation at low temperatures. Phase separation was missed in previous studies [22]. We show that it can be identified as a double peak structure in the histogram but only at low temperature and for $L \geq 10$.

V. ORDER PARAMETERS

Each of the states discussed as low temperature phases of Eq. (1) correspond to unique combinations of order parameters. At high temperatures the normal phase (N) is defined by the absence of order (either local or non-local). Whereas low temperature regimes tend to show order in either the diagonal or off-diagonal parts of the single-particle density matrix (or both as in the SS phase). This section lists the phases we find and the corresponding order parameters.

Solid order is defined by long-range oscillations in the density-density correlation function (diagonal long-range order in the density matrix) or, equivalently, peaks in the static structure factor at wavevector, \mathbf{Q} :

$$S_{\pi} \equiv N_s^{-2} \sum_{j,k} e^{i\mathbf{Q}\cdot(\mathbf{r}_j - \mathbf{r}_k)} \langle n_j n_k \rangle, \quad (4)$$

that indicate a spontaneous breaking of the sublattice symmetry. $N_s = L^3$ is the number of sites. For the large values of V considered here an oscillation of the density between sublattices is favored, $\mathbf{Q} = (\pi, \pi, \pi)$ on the simple cubic lattice.

The solid phase we discuss here is incompressible. The compressibility defines how easily the particle number fluctuates in the system, and is given by:

$$\kappa = \frac{\partial \rho}{\partial \mu} = \frac{N_s}{T} \left[\langle \hat{N}^2 \rangle - \langle \hat{N} \rangle^2 \right]. \quad (5)$$

where T is the temperature and the average particle density is given by:

$$\rho \equiv \langle \hat{N} \rangle \quad (6)$$

with:

$$\hat{N} \equiv N_s^{-1} \sum_i n_i. \quad (7)$$

The last equality in Eq. (5) shows that the compressibility is intrinsically non-local because it relates to density fluctuations across the entire system, $\langle \hat{N}^2 \rangle$.

The superfluid density describes the system’s response to external perturbations, such as translation or rotation.

TABLE I. Schematics of low temperature phases of Eq. (1) and related order parameters. A solid (blurred) sphere represents a localized (delocalized) particle. Delocalized particles represent non-zero superfluid density. The dashed square in the DS schematic shows the short-range checker-board pattern; such a pattern disappears outside the box but the box is repeated throughout the sample. The curved lines in the schematics for the PS1 and PS2 phases represent the phase separation boundary. The normal (N) and Bose-glass (BG) phases are not shown but have $S_\pi = 0$, $\rho_s = 0$, $\kappa > 0$ (no long-range order), and occur at high and low temperatures, respectively.

Phase	Order Parameters	Schematic	Phase	Order Parameters	Schematic
Solid (S)	$S_\pi > 0$, $\rho_s = 0$, $\kappa = 0$		Superfluid (SF)	$S_\pi = 0$, $\rho_s > 0$, $\kappa > 0$	
Supersolid (SS)	$S_\pi > 0$, $\rho_s > 0$, $\kappa > 0$		Disordered Solid (DS)	$S_\pi > 0$, $\rho_s = 0$, $\kappa > 0$	
Phase Separation (PS1)	$S_\pi > 0$, $\rho_s = 0$, $\kappa = 0$ $S_\pi = 0$, $\rho_s = 0$, $\kappa > 0$		Phase Separation (PS2)	$S_\pi > 0$, $\rho_s > 0$, $\kappa > 0$ $S_\pi = 0$, $\rho_s > 0$, $\kappa > 0$	

It is characterized by off-diagonal long-range order in the density matrix even in the presence of interactions. In the path-integral QMC formalism the superfluid density is given by [36]:

$$\rho_s = \frac{T\langle W^2 \rangle}{3t\rho}, \quad (8)$$

where the squared winding number is $W^2 = W_x^2 + W_y^2 + W_z^2$ and W_i is the winding number in the i th direction with $i = x, y$, or z . We find that the above order parameters adequately characterize the low-temperature phases of Eq. (1).

Table I summarizes the order parameters and the phases we find. As we vary T , t , and Δ , we find the following phases: normal, solid, superfluid, supersolid, disordered solid, and Bose-glass. The absence of order at high T signals the normal phase. The system forms a $\rho = 1/2$ solid when it has long-range diagonal order, $S_\pi > 0$, while maintaining incompressibility, $\kappa = 0$. Superfluid order is described by $\rho_s > 0$ and $\kappa > 0$. To obtain supersolid order, the system needs to have coexisting solid and superfluid orders, i.e., $S_\pi > 0$, $\rho_s > 0$, and $\kappa > 0$. The disordered solid arises in the presence of disorder. Defects lead to domains with gapless edges that leave the system compressible, i.e., $S_\pi > 0$ but with $\kappa > 0$. The Bose-glass phase occurs for large disorder strengths. It has only local superfluid order (no off-diagonal long-range order). It is compressible but exists only at low T .

We also discuss two types of phase separation. The first phase separated state, PS1, is a combination of solid order and fluctuating-Mott order found at low T and

small t , even in the absence of disorder. The Mott phase is incompressible at $T = 0$ and occurs for $\rho = 1$ (no diagonal long-range order). But we find that for $T > 0$ a fluctuating Mott (with $\rho = 1$ and $\kappa > 0$) is also possible. These phases make up the phase separated state PS1.

The second phase separated state, PS2, forms at low T but at larger t . Here the supersolid and the superfluid phase separate. These phase separated states are discussed in more detail in Sec. VII.

VI. ISING SPIN LIMIT: THE BLUME-CAPEL MODEL

The $t = 0$ limit of Eq. (1) maps into a spin-1 Ising model, the Blume-Capel model [37, 38], at low chemical potentials. We can use this mapping to gain insight into the possible phases. Previous work has shown that the Blume-Capel model exhibits phase separation even on the simple cubic lattice. This section explores the connection between the Blume-Capel model and Eq. (1).

To map Eq. (1) to a spin-1 Ising model in the dilute limit we impose a cutoff in the number of bosons per site such that n_i only takes values 0, 1, and 2. We can then define a spin-1 Ising spin variable:

$$\sigma_i = 1 - n_i, \quad (9)$$

where σ_i has values $+1, 0, -1$.

The dilute $t = 0$ limit of Eq. (1) then reduces to:

$$\frac{U}{2} \sum_i \sigma_i^2 + V \sum_{\langle ij \rangle} \sigma_i \sigma_j + \sum_i (\mu_i - \frac{U}{2} - zV) \sigma_i. \quad (10)$$

This model can be further simplified by performing a spin rotation on one of the sub lattices, i.e., $\sigma_i \rightarrow -\sigma_i$ for i on odd lattice sites. We obtain the Blume-Capel model [37, 38]:

$$H_I \equiv \frac{U}{2} \sum_i \sigma_i^2 - V \sum_{\langle ij \rangle} \sigma_i \sigma_j, \quad (11)$$

where we have omitted the staggered magnetic field term that derives from the chemical potential term in Eq. (1).

There are two phases in the translationally invariant Blume-Capel model at zero temperature. The ferromagnetic phase, with order parameters $\langle \sigma_i \rangle = 1$ and $\langle \sigma_i^2 \rangle - \langle \sigma_i \rangle^2 = 0$, arises in the $V/U \gg 1$ limit. The non-magnetic phase, $\langle \sigma_i \rangle = 0$ and $\langle \sigma_i^2 \rangle - \langle \sigma_i \rangle^2 = 1$, arises in the $V/U \ll 1$ limit. The magnetic and non-magnetic phases correspond to the solid and Mott phases in Eq. (1), respectively.

It is well known that the Blume-Capel model exhibits phase separation for $V/U \sim 1$ [39] at low T . The existence of a phase separated state in Eq. (11) on the simple cubic lattice shows that the $t \rightarrow 0$ limit of Eq. (1) should also exhibit phase separation in the dilute low T regime on the simple cubic lattice. Phase separation between the solid and Mott phase is denoted by PS1 in Table I. The mapping presented in this section therefore shows that we should expect to find phase separation (PS1) at low T in Eq. (11) even on the simple cubic lattice.

VII. PHASE SEPARATION

Sec. VI argued for phase separation in Eq. (1) in the $t \rightarrow 0$ limit using a mapping to the Blume-Capel model. In this section we use direct numerical simulation of Eq. (1) to search for phase separation, specifically PS1 and PS2 at low and high t , respectively. We detail the numerical method used to identify these states.

To detect PS1 in practice, we study the histogram of compressibility κ and S_π after multiple QMC simulations. We have done 1000 QMC simulations for the same extended Bose-Hubbard model parameters but with different initial QMC configurations. Fig. 3 shows example histograms for S_π and κ . The appearance of two peaks in the κ and S_π histograms indicate PS1 at low T . The leftmost peaks in both panels are centered at small but non-zero values because of finite-size effects. We find that the peaks trend to zero with increasing L . At low t and low T we therefore find a phase separated state that is consistent with the low T results of the Blume-Capel model [39].

We also find that the PS1 state is suppressed by thermal fluctuations. This suppression is similar to the suppression of phase separation studied in Ref. [39]. Fig. 4 shows results above the critical temperature for the PS1 state. The low-temperature ($T = 0.032$) two-peak structure in the S_π histogram disappears at the higher temperature ($T = 0.125$). Now the system has a single peak for

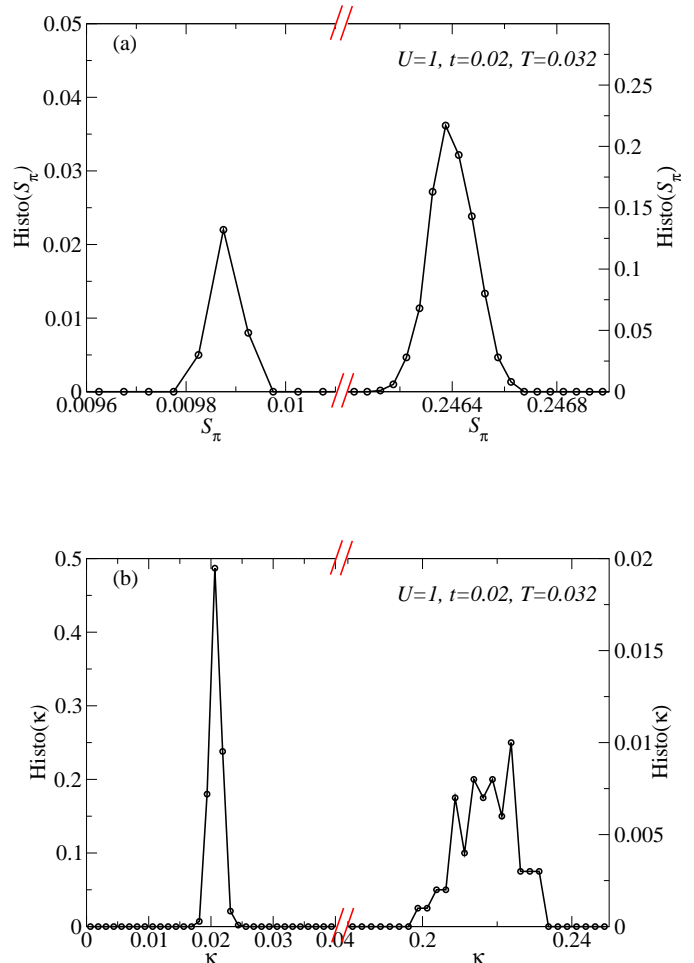


FIG. 3. The histogram for the structure factor S_π (a) and the histogram for compressibility κ (b) obtained from quantum Monte Carlo simulations of Eq. (1) in the absence of disorder ($\Delta = 0$). The pair of peaks indicate the PS1 state, a combination of solid order and fluctuating-Mott order. Here we set $U = 1$, $\mu = 0.7$, and $V = 1/z$ in Eq. (1). Simulations are performed on the simple cubic lattice with edge lengths $L = 10$.

S_π centered around $S_\pi \approx 0.23$, indicating that the system is in a pure solid phase with a well defined structure factor. Our results therefore show that the solid phase occurs only above a certain critical temperature for the PS1 state.

We find phase separation between the supersolid and the superfluid (PS2) at larger t . The PS2 state has $\rho_s > 0$ and $\kappa > 0$, as do both the superfluid and supersolid. But S_π distinguishes the superfluid and supersolid phases. We can therefore use the S_π histogram to detect the PS2 state. Fig. 5 shows an example histogram that indicates the PS2 state at a low temperature, $T = 0.05$. We find that the PS2 state is, like the PS1 state, susceptible to

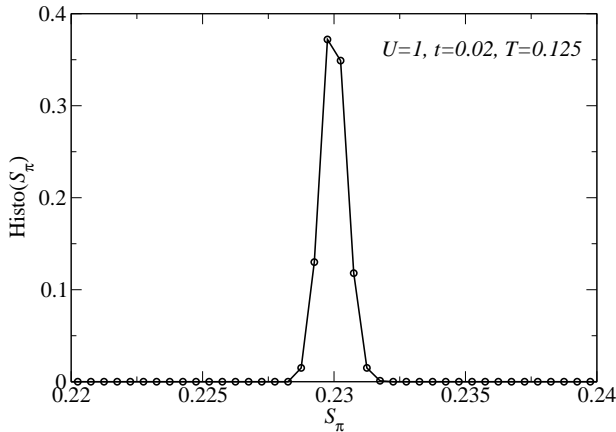


FIG. 4. The same as Fig. 3a but for a higher temperature, $T = 0.125$. The higher temperature suppresses phase separation (PS1) to leave just one phase, the solid.

thermal fluctuations. Fig. 5 also shows that the PS2 state disappears upon increasing T . Similarly, we find that the PS2 state disappears as we increase t to larger values where the SF phase forms.

We only find phase separation at large system sizes. The smallest system size showing phase separation is $L = 10$ for $\Delta = 0$. For larger disorder strengths larger system sizes are needed to see bifurcation in the QMC histograms of the order parameters.

VIII. QMC CALCULATION OF ORDER PARAMETERS

This section summarizes QMC calculations of order parameters as a function of parameters in Eq. (1). Parameter sweeps are used to qualitatively identify regions of the phase diagram with (and without) disorder. These parameter sweeps are then used in Sec. IX to find phase boundaries using finite-size scaling.

To qualitatively locate phases on the T vs. t phase diagram of Eq. (1) we scan t as well as disorder Δ . We choose four disorder strengths: $\Delta = 0.0, 0.1, 0.3,$ and 0.5 . To obtain temperature dependence we also sample the following set of temperatures: $T = 0.025, 0.05, 0.1, 0.125, 0.167, 0.2, 0.25,$ and 0.5 . We first do these simulations at $L = 10$ for our qualitative estimate.

Fig. 6 plots the order parameters of the model as a function of temperature for several different t . The top panels plot the superfluid density. We can compare all four top panels to see that for large t the disorder does not suppress the superfluid density much. We can understand this effect using the mapping to the attractive Fermi-Hubbard model where the superfluid corresponds

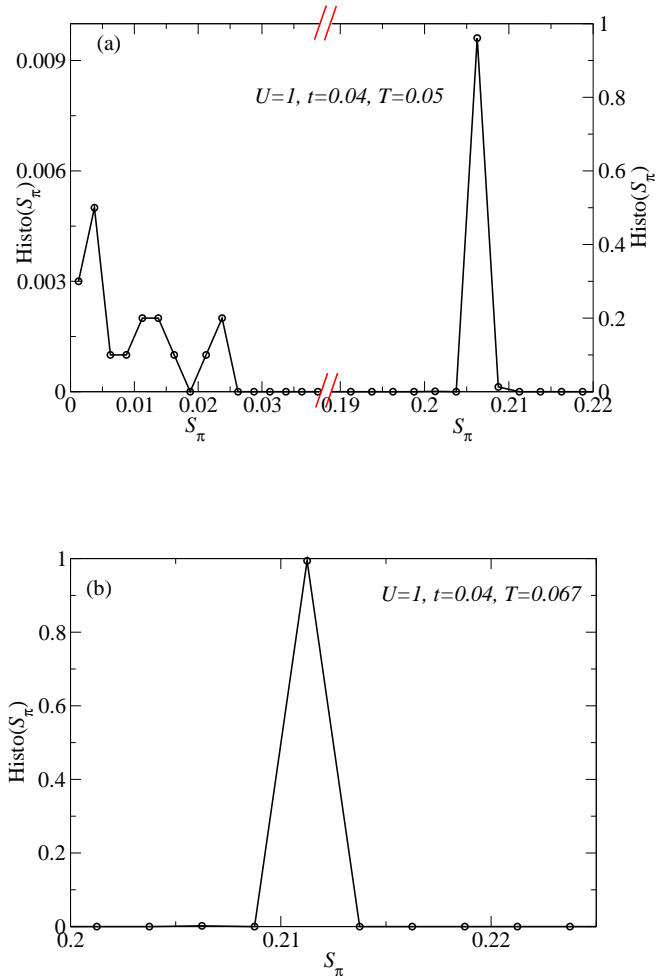


FIG. 5. Histogram for the structure factor S_π computed using quantum Monte Carlo on Eq. (1). Panel (a) is at a low temperature, $T = 0.05$, to illustrate phase separation between SF and SS phases (PS2) where we also find $\rho_s > 0$ and $\kappa > 0$ (as expected for PS2) and panel (b) is at a higher temperature, $T = 0.067$, where phase separation is suppressed and just the solid phase remains. The system size here is $L = 20$.

to an s -wave superconductor. The robustness of the superfluid found here then follows from the Anderson's theorem [40] for the robustness of s -wave superconductivity to disorder.

The middle panels in Fig. 6 plot the compressibility. Here we see that the finite size of the system keeps $\kappa > 0$ for all but the lowest t and t with $\Delta = 0$. Using finite size scaling we find that the solid phase is incompressible in the thermodynamic limit.

The bottom panels in Fig. 6 plot the structure factor. Here we see that at large t and/or T , the structure factor vanishes. This indicates that we have either the superfluid or normal phase. But for low t and low T the structure factor increases to reveal a supersolid and, for very

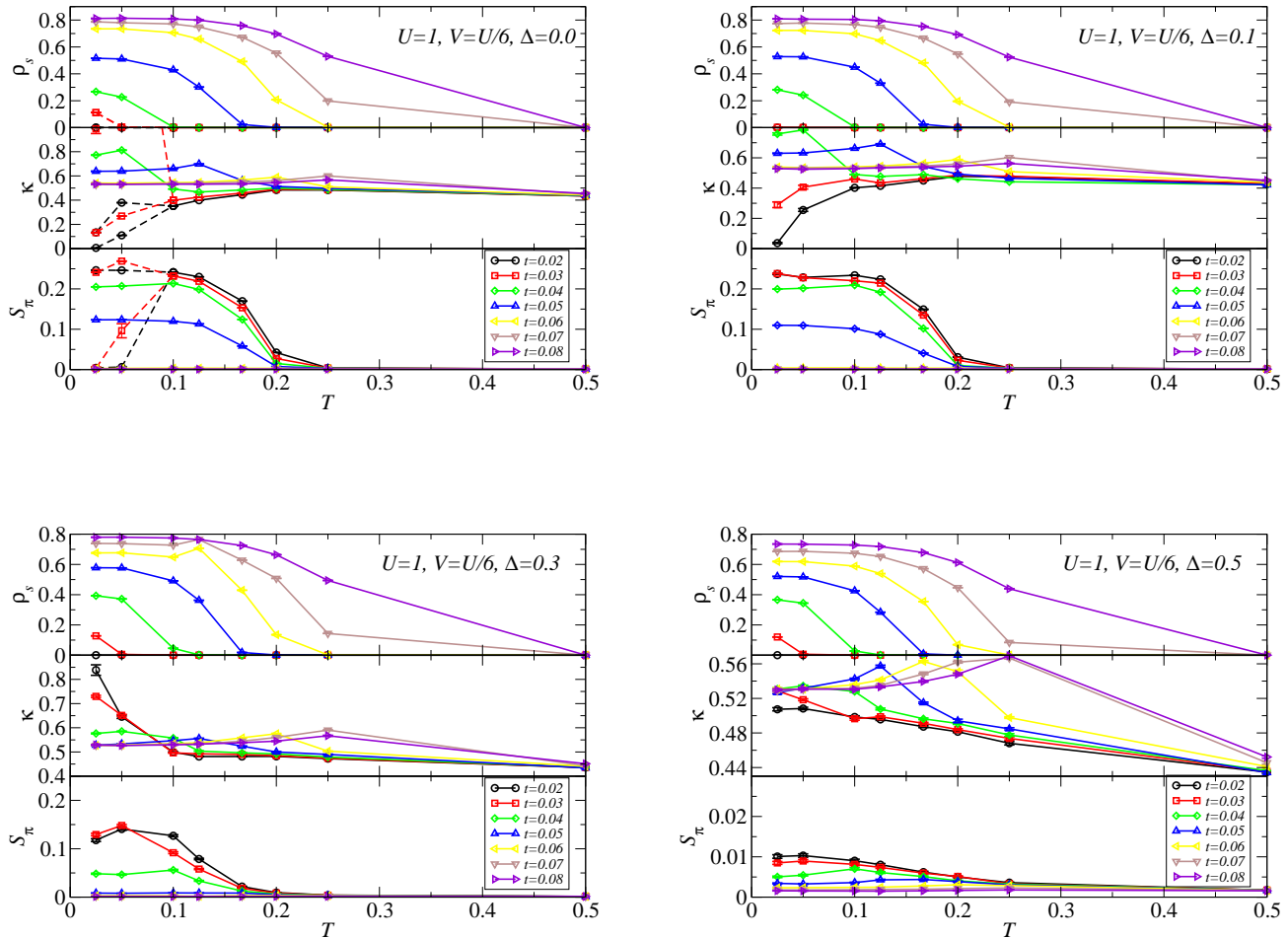


FIG. 6. Order parameters ρ_s , κ , and S_π computed as functions of temperature T and hopping t for various disorder strengths using quantum Monte Carlo on Eq. (1). Here the system size is $L = 10$. The dashed lines in the no-disorder figure, $\Delta = 0$, denote the phase separated states discussed in the text, i.e., PS1 for $t = 0.02$ (black), and PS2 for $t = 0.03$ (red). PS2 for $t = 0.04$ is not seen here, since it occurs at lower temperatures than those simulated in this graph.

low t , a pure solid. As disorder is increased to $\Delta = 0.1$ the pure solid gives way to the compressible disordered solid.

The dashed lines in Fig. 6 indicate regions where there are two peaks in the QMC distribution, i.e., phase separation. For low T the $\Delta = 0$ panel of Fig. 6 also denotes phase separation this way. For example, the $t = 0.02$ dashed black line plotting the structure factor bifurcates at low T . The two-valued dashed line signals the bimodal structure in the QMC distribution. As we increase the hopping ($t \geq 0.04$), the phase separation disappears. Phase separation is also suppressed as we increase temperatures higher than $T \sim 0.1$. At $t = 0.02$ (black dashed lines), we always have $\rho_s = 0$, but we have two distinct values of S_π and κ , respectively, signaling the first kind of phase separation, PS1, discussed above. At $t = 0.03$ (red dashed lines), we have finite ρ_s , but we again have

two distinct values of S_π and κ , respectively, signaling the second kind of phase separation, PS2. As we further increase the hopping to $t = 0.04$ (green solid lines), we see that phase separation disappears and the system assumes a supersolid phase at low T . The supersolid phase persists as we increase t to $t = 0.05$ (blue solid lines), and turns into the superfluid phase at $t = 0.06$ as the solid order is destroyed, i.e., the structure factor is suppressed.

At $\Delta = 0.1$, we find that the supersolid phase at $t = 0.03$ is destroyed. The system has $\rho_s = 0$, $\kappa > 0$ and $S_\pi > 0$, satisfying the definition of the disordered solid phase. By increasing t to $t = 0.04$, we recover the supersolid phase, which persists until $t = 0.06$. For larger t the system enters the superfluid phase. $\Delta = 0.3$ shows a similar set of transitions.

For $\Delta = 0.5$ and small t ($t = 0.02$), we have $\kappa > 0$, $\rho_s = 0$, and $S_\pi \sim 0$, which is the Bose-glass phase at low T .

As we increase the hopping to $t = 0.03$, the system turns into the superfluid at low temperatures. The superfluid phase persists as we further increase t values.

Note that the above rough determination of phase boundaries for $L = 10$ will change with system size. The critical points deduced from Fig. 6 are only approximate. Precise determination of critical points can be achieved through finite-size scalings to be discussed in Sec. IX. However, from the numerical simulations at $L = 10$, we already see the rich phase diagram contained in the disordered extended Bose-Hubbard model. Numerical simulations at $L = 10$ also serve as a rough guide to phase transitions, which will suggest parameters for a precise finite-sizing scaling analysis.

IX. FINITE-SIZE SCALING

To map out the finite temperature phase boundaries, we used QMC data to carry out finite-size scaling analyses for the order parameters. We found two distinct universality classes governing transitions: Ising and 3D XY. The Ising universality class applies to the long-range charge order/disorder transition while the 3D XY universality class applies to superfluid/non-superfluid transitions. In this section we discuss the methods we used to identify the transition points using finite size scaling relations.

Since the long-range charge order to disorder transition belongs to Ising universality class, the structure factor obeys the following scaling relation [41]:

$$S_\pi = L^{-\beta/\nu} \tilde{S}_\pi(a_1 L^{1/\nu} \tilde{t}), \quad (12)$$

where $\tilde{t} = (T - T_c)/T_c$ is the reduced temperature that measures the dimensionless distance from T to the critical temperature T_c , $\beta = 0.3265(3)$, $\nu = 0.6301(4)$, a_1 is a non-universal metric factor, and \tilde{S} is a scaling function. From Eq. (12) we see that if we plot $L^{\beta/\nu} S_\pi$ vs. T for different lattice sizes, different curves will intersect at $T = T_c$. Two example scaling figures are shown in the upper two panels of Fig. 7 for $\Delta = 0.1$.

On the other hand, the superfluid to non-superfluid transition belongs to the 3D XY universality class, and the superfluid density scaling satisfies the following scaling relation [42]:

$$\rho_s = L^{-(d-2)} \tilde{\rho}_s(a_2 L^{1/\nu} \tilde{t}), \quad (13)$$

where $\tilde{\rho}_s$ is a scaling function, $d = 3$ is system dimension, and a_2 is a non-universal metric factor.

In 3D, we can plot $L\rho_s$ vs. T for different lattice sizes. Different curves again intersect at $T = T_c$ for the transition. The lower two panels of Fig. 7 show example finite-size scaling analyses of ρ_s for disorder strength $\Delta = 0.1$. We have checked that the $L = 6 - 10$ data are sufficient to give accurate critical points by including larger system sizes ($L \leq 20$) for select parameters.

Using these scaling relations we are able to precisely locate phase transition lines to construct a phase diagram. We have not been able to use finite size scaling to identify phase transition lines for phase separated states because scaling relations for these phases are unknown. To estimate the critical temperature for the phase separated states we use the critical temperature for a single large system size.

X. PHASE DIAGRAMS

This section culminates the results and methods presented in previous sections to construct phase diagrams of Eq. (1). Finite-size scaling of the superfluid stiffness and the structure factor are used to find finite temperature critical points for the solid, supersolid, and superfluid phases. We find that the supersolid is present at intermediate hopping even in the presence of disorder. But we find two surprising results: 1) The low temperature part of the phase diagram is dominated by phase separation. This implies the putative quantum critical point between the solid and supersolid at this chemical potential is masked by phase separation. 2) Disorder suppresses phase separation to reveal a phase diagram that is at first glance similar to what has been expected from mean field studies. But Griffiths effects make the phase diagram fundamentally different from what is expected from zero-disorder cases.

Fig. 8 plots the phase diagram of Eq. (1) in the absence of disorder as determined by QMC. Here squares and circles plot the critical temperature determined by finite-sized scaling of the structure factor and the stiffness, respectively. Here we see that the solid and superfluid dominate at small and large hopping, respectively. The supersolid is found at intermediate hoppings.

The vertical dashed line in Fig. 8 indicates an expected phase boundary. Our conclusion here is based on finite size data without extrapolation. Increasing system size drives the critical temperature to zero for $t \gtrsim 0.0525$. Here we were not able to resolve the critical temperature uniquely given our method because the phase boundary is nearly vertical here.

The diamonds (joined by a dotted line) in Fig. 8 show the critical temperature for phase separated states. The points were determined at our largest system size available, $L = 20$. Below these critical temperatures the structure factor histogram obtained from QMC bifurcates. Above these temperatures the histograms center around a single value. Finite-sized scaling relations are not known for the phase separated states. We see phase separation for several L but we have discerned no clear trend.

Fig. 8 shows that at zero disorder the extended Bose Hubbard model, Eq. (1), on the simple cubic lattice is dominated by phase separation at low temperatures. Here, in contrast to what has been expected from mean field theory and QMC studies [11, 14, 22], phase separa-

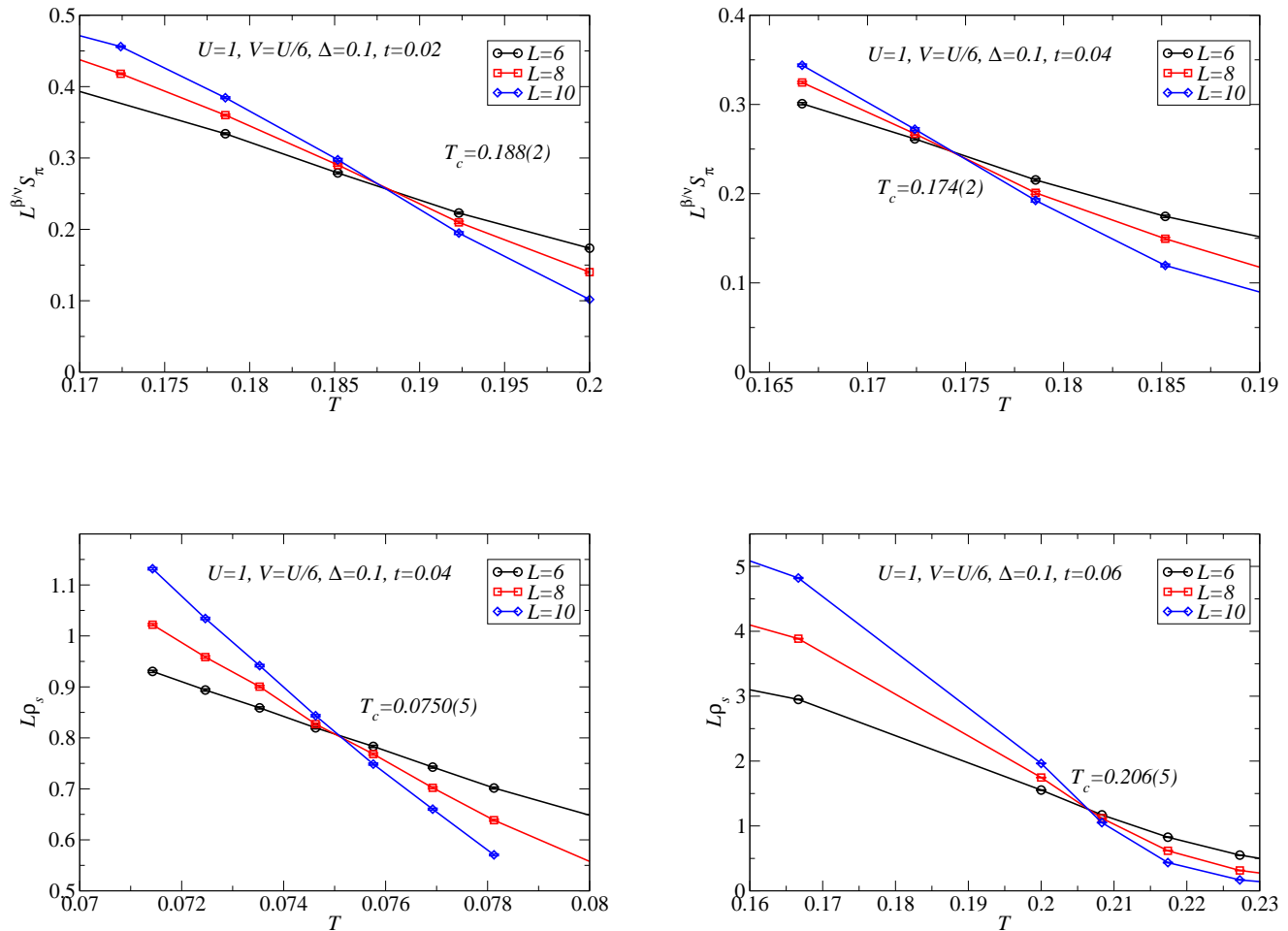


FIG. 7. Example rescaled order parameters plotted as a function of temperature computed using quantum Monte Carlo on Eq. (1). The crossings of the rescaled structure factor and superfluid density allow determination of the critical temperatures for order parameters S_π and ρ_s , respectively.

tion sets in even at $T = 0$ to prevent the formation of a quantum critical point between the solid and the supersolid phase. As temperature is increased, thermal fluctuations apparently destroy the domain wall responsible for phase separation to reveal uniform solid and supersolid phases.

Figs. 9 and 10 plot the same as Fig. 8 but in the presence of disorder. We find that increasing spatial disorder tends to suppress phase separation while leaving the other phases intact. Fig. 11 shows that the structure factor QMC histogram at $\Delta = 0.3$ acquires a range of values, as opposed to two distinct peaks as presented in Sec. VII. The absence of a zero in the histogram prevents averaging. We cannot define a clear phase separated state although the two peaks do show a trend towards phase separation. We therefore conclude that phase separation is suppressed here.

Fig. 10 shows that by increasing disorder we arrive at

a phase diagram with no phase separation, as expected from previous work at zero disorder [11, 14, 22]. But there are important differences. Our finite size simulations exclude Griffiths effects which arise because of rare disorder configurations with strong contributions to averaging. Finite size simulations miss these rare regions. But Griffiths effects should be particularly important in the thermodynamic limit near phase boundaries separating incompressible and compressible phases [23, 24]. The solid and supersolid are incompressible and compressible, respectively. Figs. 9 and 10 therefore omit the quantum Griffiths phase which, according to the theorem of inclusions [23], must separate these two phases.

We have also studied the phase diagram for the case with strong disorder, $\Delta = 0.5$. Here we find a Bose glass at low T and low t . At $T = 0$ we find a Bose glass for $t \lesssim 0.021$ and a superfluid for $t \gtrsim 0.021$.

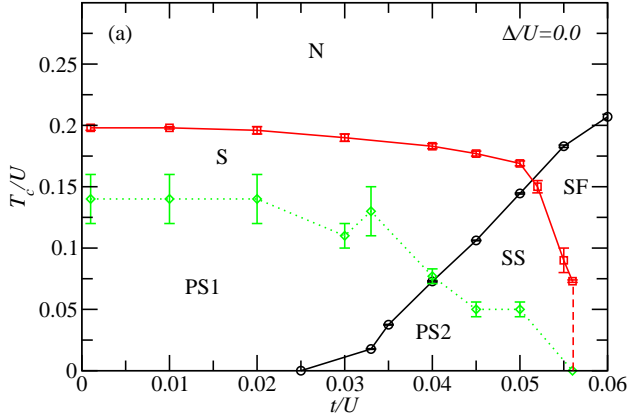


FIG. 8. Critical temperatures of the extended Bose Hubbard model, Eq. (1), computed using quantum Monte Carlo for no disorder. We have set $\mu = 0.7$ and $V = 1/z$. Squares result from the S_π scaling analysis [Eq. (12)] and circles are from the ρ_s scaling analysis [Eq. (13)]. Diamonds (determined from $L = 20$ simulations) show the phase separation critical temperature. Below the diamonds the system phase separates. Lines are a guide to the eye.

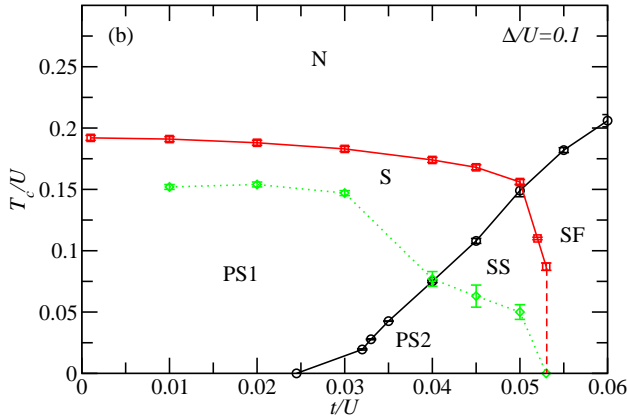


FIG. 9. The same as Fig. 8 but for $\Delta = 0.1$.

XI. DISORDER ENHANCED SUPERSOLIDITY

The addition of disorder can, counterintuitively, enhance supersolidity. Previous work [25] used QMC and mean field theory to show that the addition of disorder enhances supersolidity in Eq. (1). The mechanism required disorder to create pathways for the superfluid to percolate across the entire sample while allowing diagonal long-range order to persist. (This is related to disorder enhanced superfluidity found in the Bose-Hubbard model

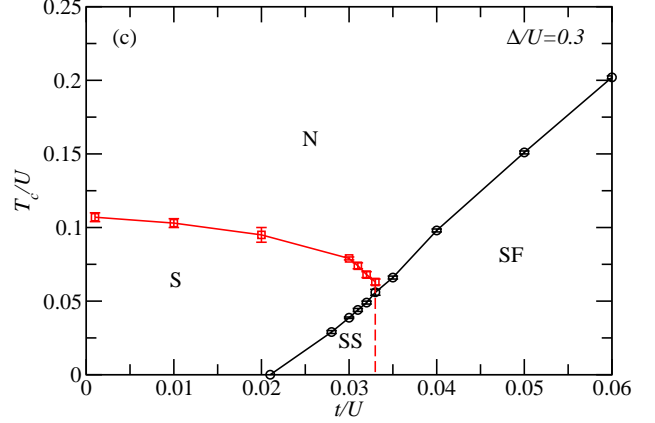


FIG. 10. The same as Fig. 8 but for $\Delta = 0.3$. Here we find no phase separation in our simulations. This phase diagram resembles the previously expected phase diagram (Fig. 1b) because phase separation is suppressed.

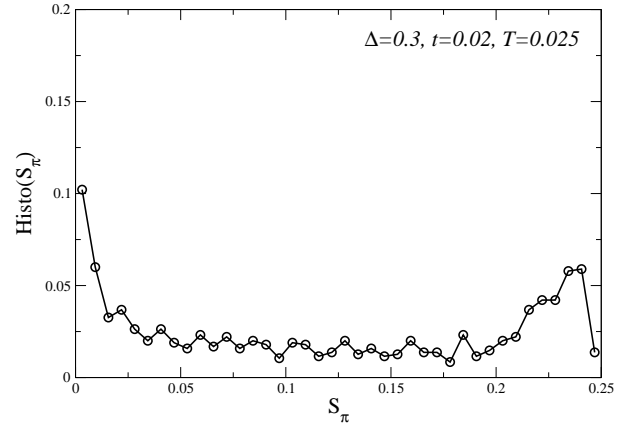


FIG. 11. Histogram for the structure factor S_π computed using quantum Monte Carlo on Eq. (1) showing suppression of phase separation by disorder. Here we set $U = 1$, $\mu = 0.7$, $V = 1/z$, and disorder strength $\Delta = 0.3$. The strong disorder prevents zeroing in the histogram and therefore prevents averaging needed to define a phase separation state.

($V = 0$) [24, 43, 44]). Ref. 25 showed that the order parameters increased with disorder for finite sized systems. This section uses finite-sized scaling to show that disorder increases the critical temperature of the supersolid phase in the thermodynamic limit.

To further explore the effect of disorder in the SS phase, we use finite-size scaling to extract critical temperatures for SS for various disorder strength ($\Delta = 0, 0.1, 0.2, 0.3$). Finite-size scaling is performed for lat-

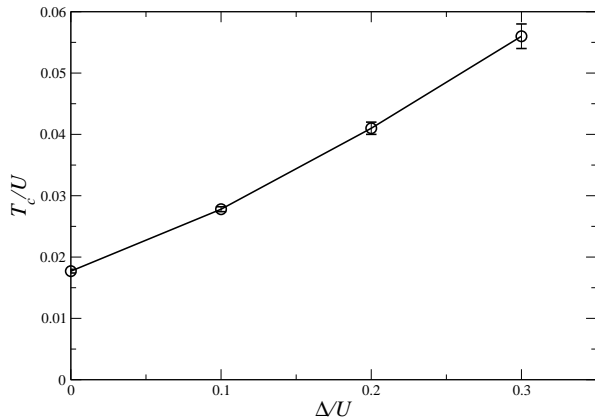


FIG. 12. Circles plot the critical temperature of the supersolid phase as a function of disorder strength computed using quantum Monte Carlo on Eq. (1) along with finite size scaling. These results show that disordered enhances critical temperature for the supersolid phase. Here we set $U = 1$, $\mu = 0.7$, $V = 1/z$, and $t = 0.33$.

tice sizes $L = 6, 8, 10$. Although there is PS2 in this parameter regime, we stay in the SS phase by performing S_π average for resulting configurations where S_π assumes values far away from zero.

Fig. 12 shows an enhancement of the critical temperature for the SS phase from $T_c \sim 0.02$ to $T_c \sim 0.06$ as we increase the disorder strength from $\Delta = 0.0$ to $\Delta = 0.3$. It is worth noting that an approximate 3-fold increase of the SS critical temperature is achieved by increasing disorder. Fig. 12 is consistent with results presented in Ref. 25 but carries the calculation into the thermodynamic limit with an explicit calculation of T_c . T_c drops quickly for larger disorder strengths, e.g., at $\Delta = 0.5$ we find $T_c = 0.038(1)$.

The disorder enhanced supersolid can be understood in a mean-field percolation picture [25]. Consider the pure solid phase near the solid-supersolid phase boundary in the absence of disorder. The gap in the solid phase prevents density fluctuations and therefore suppresses inter-site tunneling needed for concomitant superfluidity. The addition of site disorder allows tunneling between sites with sufficiently strong disorder. If the collection of bonds allowing tunneling percolates across the sample, then a superfluid forms. In this way the superfluid has been found to be triggered by the addition of disorder in Bose-Hubbard models [23, 24, 43, 45, 46]. But here the background solid remains intact leading to a supersolid that has been triggered by the addition of disorder.

XII. SUMMARY

We have used quantum Monte Carlo to study the extended Bose-Hubbard model with disorder on the simple cubic lattice. We have computed the finite temperature phase diagram at fixed chemical potential. We find that phase separation dominates the low temperature part of the phase diagram in the absence of disorder. This contrasts with previous work where no phase separation was found [22]. We have also found that increasing disorder tends to suppress phase separation. The quantum critical point expected between the solid and supersolid was not found because of an incipient phase separated state similar to results found in the Fermi-Hubbard model [47]. Overall our results show that disorder and thermal fluctuations favor the supersolid phase, in contrast to lower dimensions where disorder suppresses the supersolid [21]. Our results show that in 3D the supersolid should be more robust.

ACKNOWLEDGMENTS

We thank M. Troyer for helpful input. We acknowledge support from AFOSR (FA9550-11-1-0313).

-
- [1] G. V. Chester, Phys. Rev. A **2**, 256 (1970).
 - [2] M. Boninsegni and N. V. Prokofev, Rev. Mod. Phys. **84**, 759 (2012).
 - [3] E. Kim and M. Chan, Nature **427**, 225 (2004).
 - [4] D. Y. Kim and M. H. W. Chan, Phys. Rev. Lett. **109** (2012).
 - [5] T. Matsubara and H. Matsuda, Prog. of Theor. Phys. **16**, 569 (1956).
 - [6] H. Matsuda and T. Tsuneto, Prog. Theor. Phys. Suppl. **46**, 411 (1970).
 - [7] K.-S. Liu and M. E. Fisher, J. Low Temp. Phys. **10**, 655 (1972).
 - [8] K. Goral, L. Santos, and M. Lewenstein, Phys. Rev. Lett. **88**, 170406 (2002).
 - [9] H. Buchler and G. Blatter, Phys. Rev. Lett. **91**, 130404 (2003).
 - [10] V. W. Scarola and S. Das Sarma, Phys. Rev. Lett. **95**, 033003 (2005).
 - [11] V. W. Scarola, E. Demler, and S. Das Sarma, Phys. Rev. A **73**, 051601 (2006).
 - [12] I. Bloch, J. Dalibard, and W. Zwerger, Rev. Mod. Phys. **80**, 885 (2008).
 - [13] S. Baier, M. J. Mark, D. Petter, K. Aikawa, L. Chomaz, Z. Cai, M. Baranov, P. Zoller, and F. Ferlaino, (2015), arxiv:1507.03500.
 - [14] A. van Otterlo, K. Wagenblast, R. Baltin, C. Bruder, R. Fazio, and G. Schon, Phys. Rev. B **52**, 16176 (1995).
 - [15] E. Roddick and D. Stroud, Phys. Rev. B **51**, 8672 (1995).

- [16] R. Micnas, J. Ranninger, and S. Robaszkiewicz, *Rev. Mod. Phys.* **62**, 113 (1990).
- [17] S. H. Blanton, R. T. Collins, K. H. Kelleher, L. D. Rotter, Z. Schlesinger, D. G. Hinks, and Y. Zheng, *Phys. Rev. B* **47**, 996 (1993).
- [18] P. Sengupta, L. P. Pryadko, F. Alet, M. Troyer, and G. Schmid, *Phys. Rev. Lett.* **94**, 207202 (2005).
- [19] S. Wessel and M. Troyer, *Phys. Rev. Lett.* **95**, 127205 (2005).
- [20] K. Bernardet, G. Batrouni, and M. Troyer, *Phys. Rev. B* **66**, 054520 (2002).
- [21] Y. Imry and S. Ma, *Phys. Rev. Lett.* **35**, 1399 (1975).
- [22] K. Yamamoto, S. Todo, and S. Miyashita, *Phys. Rev. B* **79**, 094503 (2009).
- [23] L. Pollet, N. V. Prokof'ev, B. V. Svistunov, and M. Troyer, *Phys. Rev. Lett.* **103**, 140402 (2009).
- [24] V. Gurarie, L. Pollet, N. V. Prokof'ev, B. V. Svistunov, and M. Troyer, *Phys. Rev. B* **80**, 214519 (2009).
- [25] B. M. Kumburi and V. W. Scarola, *Phys. Rev. B* **85**, 020501 (2012).
- [26] M. Fisher, P. Weichman, G. Grinstein, and D. Fisher, *Phys. Rev. B* **40**, 546 (1989).
- [27] S. Robaszkiewicz, R. Micnas, and K. A. Chao, *Phys. Rev. B* **23**, 1447 (1981).
- [28] S. Robaszkiewicz, R. Micnas, and K. A. Chao, *Phys. Rev. B* **24**, 1579 (1981).
- [29] J. E. Hirsch and D. J. Scalapino, *Phys. Rev. B* **32**, 5639 (1985).
- [30] E. Dagotto, A. Moreo, and U. Wolff, *Phys. Lett. B* **186**, 395 (1987).
- [31] C. M. Varma, *Phys. Rev. Lett.* **61**, 2713 (1988).
- [32] R. T. Scalettar, E. Y. Loh, J. E. Gubernatis, A. Moreo, S. R. White, D. J. Scalapino, R. L. Sugar, and E. Dagotto, *Phys. Rev. Lett.* **62**, 1407 (1989).
- [33] K. Aryanpour, T. Paiva, W. E. Pickett, and R. T. Scalettar, *Phys. Rev. B* **76**, 184521 (2007).
- [34] A. W. Sandvik, *Phys. Rev. B* **59**, R14157 (1999).
- [35] O. Syljuasen and A. Sandvik, *Phys. Rev. E* **66**, 046701 (2002).
- [36] E. L. Pollock and D. M. Ceperley, *Phys. Rev. B* **36**, 8343 (1987).
- [37] M. Blume, *Phys. Rev.* **141**, 517 (1966).
- [38] H. Capel, *Physica* **32**, 966 (1966).
- [39] M. Blume, V. J. Emery, and R. B. Griffiths, *Phys. Rev. A* **4**, 1071 (1971).
- [40] P. Anderson, *J. Phys. Chem. Solids* **11**, 26 (1959).
- [41] V. Privman and M. E. Fisher, *Phys. Rev. B* **30**, 322 (1984).
- [42] M.-C. Cha, M. P. A. Fisher, S. M. Girvin, M. Wallin, and A. P. Young, *Phys. Rev. B* **44**, 6883 (1991).
- [43] W. Krauth, N. Trivedi, and D. Ceperley, *Phys. Rev. Lett.* **67**, 2307 (1991).
- [44] F. Lin, E. S. Sorensen, and D. M. Ceperley, *Phys. Rev. B* **84**, 094507 (2011).
- [45] K. Sheshadri, H. R. Krishnamurthy, R. Pandit, and T. V. Ramakrishnan, *Phys. Rev. Lett.* **75**, 4075 (1995).
- [46] L. Dang, M. Boninsegni, and L. Pollet, *Phys. Rev. B* **79**, 214529 (2009).
- [47] D. Galanakis, E. Khatami, K. Mikelsons, A. Macridin, J. Moreno, D. A. Browne, and M. Jarrell, *Phil. Trans. R. Soc. B* **369**, 1670 (2011).